THESIS

FABRICATION OF OMNIPHOBIC AND SUPEROMNIPHOBIC SURFACES

Submitted by

Anudeep Pendurthi

Department of Mechanical Engineering

In partial fulfillment of the requirements

For the Degree of Master of Science

Colorado State University

Fort Collins, Colorado

Fall 2017

Master's Committee:

Advisor: Arun K. Kota
Co-Advisor: Azer P. Yalin

Matt J. Kipper

ABSTRACT

FABRICATION OF OMNIPHOBIC AND SUPEROMNIPHOBIC SURFACES

Superomniphobic surfaces (i.e., surfaces that are extremely repellent to both high surface tension liquids like water and low surface tension liquid like oils and alcohols) can be fabricated through a combination of surface chemistry that imparts low solid surface energy and a re-entrant surface texture. Recently, surface texturing with lasers has received significant attention because laser texturing is scalable, solvent-free, and can produce a monolithic texture (i.e., a texture that is an integral part of the surface unlike a coating that is deposited on the underlying substrate) on virtually any material.

In this work, we fabricated nanostructured omniphobic and superomniphobic surfaces with stainless steel 430, stainless steel 316, stainless steel 304, titanium, aluminum and glass surfaces using a simple, inexpensive and commercially available CO_2 laser engraver. Further, we demonstrated that the nanostructured omniphobic and superomniphobic surfaces fabricated using our laser texturing technique can be used to design patterned surfaces, surfaces with discrete domains of the desired wettability and on-surface microfluidic devices. Systematic experiments were conducted to evaluate the importance of various laser parameters to fabricate these omniphobic and superomniphobic surfaces. Also, the performance of these surfaces under adverse acidic and basic conditions was evaluated systematically.

In addition to surface texturing with lasers, in this work, we also report a simple and versatile method to fabricate superomniphobic glass microfiber paper by growing silicone nanofilaments using trichloromethylsilane (TCMS).

ACKNOWLEDGEMENTS

I would like to express my special thanks of gratitude to Dr. Arun Kota who gave me the golden opportunity to do this wonderful research in the field of Surface Science. I would like to thank Sanli Movafaghi for all the support with X-ray Photoelectron Spectroscopy (XPS) and Scanning Electron Microscopy (SEM). I would like to thank all the students in Kota Research Group, Hamed Vahabi, Wei Wang, Lewis Boyd, Sravanthi Vallabhuneni, Matthew Scott and Matt Cackovic for providing engaging discussions and illuminating instructions during our regular group meetings. I would like to thank Dr. Azer P Yalin and Soran Shadman for all their valuable time in helping me to pursue this research in a commendable way. My sincere thanks to Scott Kreider from the Department of Art and Art History at Colorado State University, for all his support to this research. Thank you to the thesis committee for providing guidance and suggestions during the research process. I would also like to show my gratitude to Colorado Office of Economic Development and International Trade for financial support under the Advanced Industry Accelerator Grant Program.

TABLE OF CONTENTS

1 INTRODUCTION OF WETTABILITY

1.1 Contact Angle

Surface wettability is usually characterized by the contact angles and contact angle hysteresis[1,2] of liquids. Thomas Young defined equilibrium contact angle of any liquid droplet on non-textured (e.g., smooth) surfaces as:

$$\mathrm{Cos}(\theta_Y) = \frac{\gamma_{SV} - \gamma_{SL}}{\gamma_{LV}} \quad (1)$$

where, γ_{SV} is the solid surface energy, γ_{LV} is the liquid surface tension and γ_{SL} is the solid-liquid interfacial energy. This equation arises from the energy balance for a liquid droplet contacting a flat, non-textured and non-reactive solid surface, and can be visualized in Figure 1 with the contact angle being the angle between the tangent to the liquid-vapor interface and the tangent to the solid-liquid interface at the triple phase contact line, measured through the liquid:

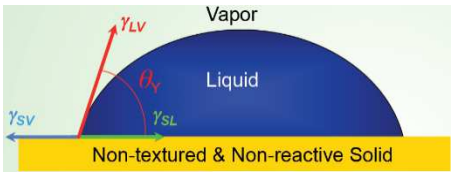

Figure 1: Schematic of energy balance at the triple-phase contact point for a liquid drop on a flat surface (Image reproduced with permission from Dr. Kota's "Bio Inspired Surfaces" lecture).

A surface that has a young's contact angle for both high and low surface tension liquid droplets greater than 90^o ($\theta > 90^o$) is considered omniphobic and a surface that has young's contact angle for both high surface tension and low surface tension liquids less than 90^o ($\theta < 90^o$) is considered omniphillic. According to the Young's equation, a liquid droplet will have higher contact angles on low surface energy materials and a liquid droplet will have lower contact angles on higher surface energy materials. Thus, lower surface energy materials are preferred to fabricate superomniphobic surfaces.

1.2 Contact Angle Hysteresis

The contact angle hysteresis (CAH) for a surface is another significant parameter for characterization of surface wettability[3-13]. The liquid droplets will not interact on all parts of a surface due to the contaminants, roughness and surface chemistry leading to the difference in contact angles on the same surface. Contact angle hysteresis is the difference between the advancing and receding contact angles for a surface (Figure 2)[14,15]. Superomniphobic surfaces will have low contact angle hysteresis.

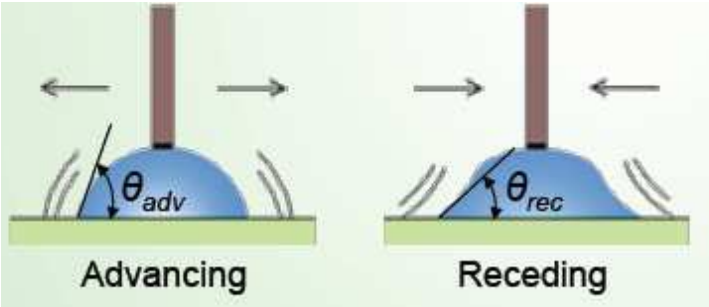

Figure 2: Schematic of advancing and receding contact angle measurements for a liquid drop (Image reproduced with permission from Dr. Kota's "Bio Inspired Surfaces" lecture).

1.3 Sliding/Roll Off Angle

Sliding/Roll Off Angle is the minimum angle by which a solid surface has to be titled relative to horizontal for a liquid droplet to slide off or roll off from the solid surface. In 1962, Furmidge provided an equation to estimate the sliding/roll off angle of a liquid droplet on a surface by force balance on a sliding/rolling droplet. The liquid droplet will start to slide/roll off when the surface is tilted to an angle α. The sliding/roll off angle can be approximated with Furmidge's equation:

$$\sin(\alpha) = \frac{\gamma_{LV} w(\cos\theta_R + \cos\theta_A)}{\rho g V} \qquad (2)$$

Where w is the width of triple phase contact line, v is the volume of the liquid droplet, ρ is the density of liquid droplet, and g is the gravitational acceleration.

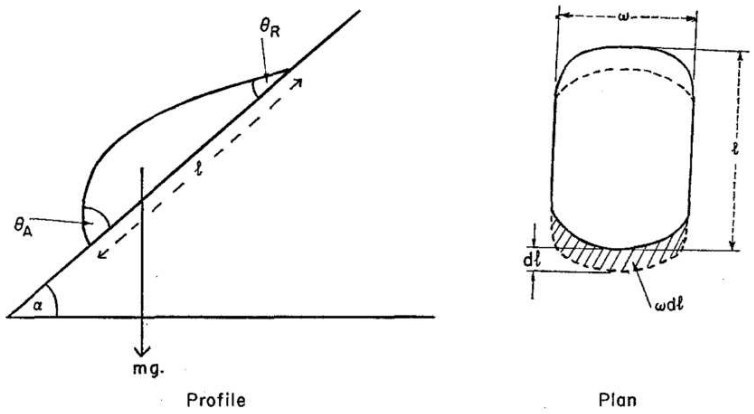

FIG. 4. Profile and plan view of drop during sliding without acceleration.
θ_A—advancing contact angle
θ_R—receding contact angle
l—overall length of drop
w—overall width of drop

Furmidge, 1962, 316

Figure 3: Schematic of drop during sliding (Image Reproduced with permission from [15]).

1.4 Wenzel State

In 1936, Robert Wenzel provided the earliest analyses of a liquid droplet sitting on a textured surface[16]. According to Wenzel, any solid surface will have a greater surface area than a perfectly flat surface due to surface roughness. The surface roughness can be characterized by roughness factor, r, which is the ratio of actual solid surface area to the geometric surface area.

$$r = \frac{SA_{Actual}}{SA_{Projected}} \tag{3}$$

The availability of smooth surfaces (i.e., roughness factor =1) is not possible. So, any surface ideally has a roughness factor of greater than unity. Further analysis by Wenzel considers the effect of that increased surface area on contact angles of liquids when the liquid completely wets the surface. The apparent contact angles of liquid droplets as a function of roughness factor, *r*, and the young's contact angle, θ:

$$\mathrm{Cos}(\theta_W^*) = r\cos(\theta) \tag{4}$$

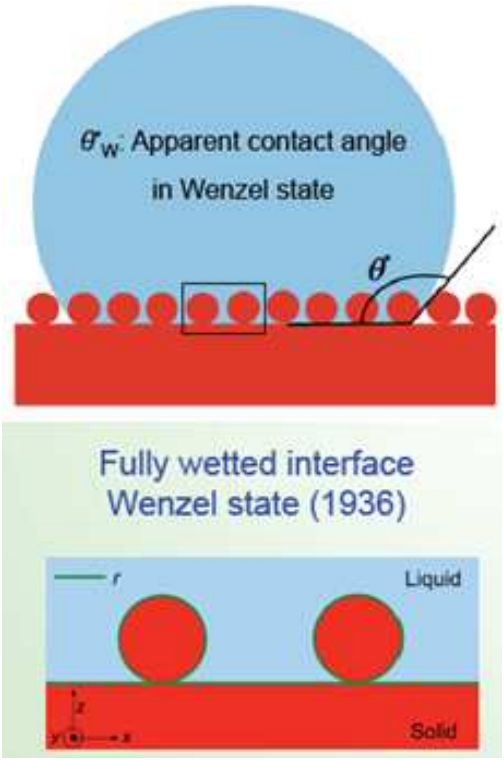

Figure 4: Schematic of a liquid drop in the Wenzel state on a textured surface (Image reproduced with permission from Dr. Kota's "Bio Inspired Surfaces" lecture).

1.5 Cassie-Baxter State

Cassie and Baxter expanded on Wenzel's work by considering that surfaces are not always completely wet, but rather textured surfaces can have air trapped within the texture. When a drop partially wets a textured surface in the Cassie-Baxter state, the apparent contact angle θ^*_{CB} on a partially-wetted textured surface:

$$cos\theta^*_{CB} = f_{SL}cos\theta + f_{LV}cos\pi \quad (5)$$

where f_{SL} is the area fraction of the solid-liquid interface and f_{LV} is the area fraction of the liquid-vapor interface of a liquid droplet in the Cassie-Baxter state. These parameters are geometrically-dependent, as calculations for their values are based on repeating unit cells for the texture. From Cassie-Baxter equation, it is evident that the increase in liquid-vapor interfacial area fraction will increase the contact angles of the liquid droplet.

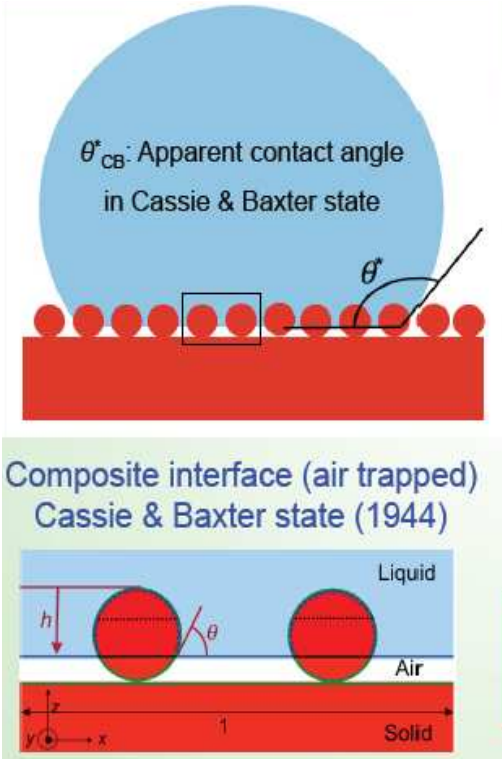

Figure 5: Schematic of a liquid drop in the Cassie-Baxter state on a textured surface (Image reproduced with permission from Dr. Kota's "Bio Inspired Surfaces" lecture).

1.6 Design of Superomniphobic Surfaces

Superhydrophobic surfaces can repel water and aqueous liquids, however, they typically cannot repel low surface tension liquids (e.g., oils) because lower surface tension liquids have lower contact angles on a given solid surface compared to higher surface tension liquids. The Cassie-Baxter state is preferred for designing superomniphobic surfaces because the air pockets reduce the solid-liquid contact area fraction and result in higher apparent advancing contact angles θ^*_{adv}, higher apparent receding contact angles θ^*_{rec}, and lower contact angle hysteresis. However, superomniphobicity requires a specific type of texture called re-entrant (i.e., multivalued surface topography, see Figure 6a). The re-entrant texture allows a droplet to adopt a nanoscale contact

angle < 90° on the surface which is necessary for superomniphobicity because low surface tension liquids have Young's contact angle $\theta < 90°$ on virtually all surfaces.

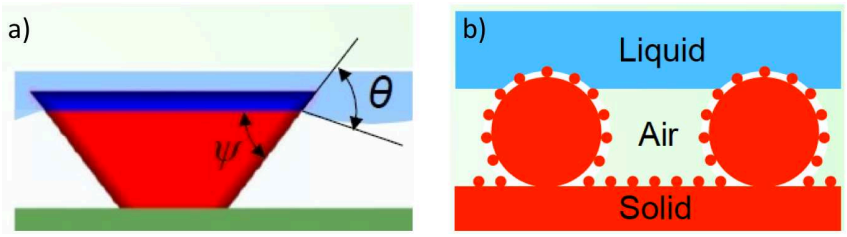

Figure 6: a) Surface texture with multivalued surface topography, can be superomniphobic b) Hierarchically textured surface (Image reproduced with permission from Dr. Kota's "Bio Inspired Surfaces" lecture.)

The presence of air pockets can be further increased by employing hierarchically textured surfaces (see Figure 6b), which have multiple length scales of texture. These hierarchically textured surfaces will have two or more length scales of textures (e.g., nano textured features superimposed on micro textured features). These hierarchically structured textures reduce the solid-liquid interfacial area fraction, which results in higher apparent advancing contact angles θ^*_{adv}, higher apparent receding contact angles θ^*_{rec}, and lower contact angle hysteresis. A surface is considered to be superomniphobic when apparent contact angle >150° and contact angle hysteresis is low for both high surface tension liquids and low surface tension liquids (e.g., oils) [17-19].

1.7 Summary

With these fundamentals, many superomniphobic surfaces have been prepared by varying texturing and surface chemistry[20-28]; however, the durability of these surfaces is a continual challenge given the importance of maintaining one or more length scales of texture. Metals are common materials for industrial application due to their high strength and durability, so work has been done to make metallic surfaces highly repellent. This work primarily focuses on fabricating omniphobic and superomniphobic stainless steel 430, stainless steel 316, stainless steel 304, aluminum, titanium, and glass surfaces in a cost-effective and simple manner using inexpensive

CO_2 laser systems. Also, we have presented a simple and versatile technique to fabricate silicone nanofilaments on glass microfiber paper surfaces to make them superomniphobic.

2 FABRICATION OF NANOSTRUCTURED OMNIPHOBIC AND SUPEROMNIPHOBIC SURFACES WITH INEXPENSIVE CO_2 LASER ENGRAVER

2.1 Background

Super-repellent surfaces can be broadly classified as superhydrophobic surfaces (i.e. Surfaces that are extremely repellent to high surface tension liquids like water) and superomniphobic surfaces (i.e. Surfaces that are extremely repellent to both high surface tension liquids like water and low surface tension liquid like oils)[17,19-22,29-32]. Super-repellent surfaces can be fabricated by combining a surface chemistry that imparts low solid surface energy with an appropriate surface texture[2,27,33-37]. Recently, fabrication of superhydrophobic surfaces via surface texturing with lasers has received significant attention[38-50] because laser texturing is scalable, solvent-free, and can produce a monolithic texture (i.e. a texture which is an integral part of the surface unlike a coating that is deposited on the underlying substrate) on virtually any material. However, there are no reports of superomniphobic surfaces fabricated via laser texturing. Further, most reports of superhydrophobic surfaces fabricated via laser texturing have employed expensive nanosecond or femtosecond lasers[38,40,41,44,45,48,49,51-54]. In this work, we present nanostructured superomniphobic surfaces fabricated via laser texturing with an inexpensive CO_2 laser engraver. We demonstrate that our simple, inexpensive, scalable and solvent-free laser texturing technique allows fabrication of superomniphobic (or omniphobic) surfaces, gradient wettability surfaces, and droplet manipulation tracks with a wide variety of materials.

2.2 Materials/Methods/Experiments

2.2.1 Fabrication of Textured Surfaces via Laser Ablation

Prior to laser ablation, all samples were cleaned by sonication in acetone and ethanol, dried with nitrogen. The laser ablation was conducted using a commercially available, quasi-continuous laser system with a central wavelength of 10.6 μm (Epilog Legend 36EXT). The laser was focused onto the sample with a ~127 μm beam diameter using a 51 mm focal length lens. The laser ablation was conducted over the desired area with powers up to 120 W and raster speeds up to 210 cm/s. The laser power and laser raster speed that resulted in the maximum liquid repellency for a variety of materials are summarized in Table 1.

Table 1: Laser power and laser raster speed for achieving maximum liquid repellency for different materials.

Surface	Laser Power (W)	Laser Raster Speed (cm/s)	Liquid Repellency
Stainless Steel 430	120	2	Superomniphobic
Stainless Steel 316	120	2	Superomniphobic
Stainless Steel 304	120	2	Omniphobic
Titanium	84	2	Omniphobic
Aluminum	84	2	Omniphobic
Glass	84	100	Omniphobic

2.2.2 Vapor Phase Silanization

The laser textured surfaces were subsequently modified via vapor phase silanization at 120°C for 1 hour using 200 μL of heptadecafluoro-1,1,2,2-tetrahydrodecyl trichlorosilane (Gelest) to impart low solid surface energy ($\gamma_{sv} \approx 10$ mN/m).

2.2.3 Characterization of Surface Morphology and Surface Roughness

The surfaces were imaged using a scanning electron microscope (JEOL JSM-6500F) at 15 kV to determine the surface morphology. The root mean square roughness R_{rms} of the surfaces was measured using an optical profilometer (Zygo Zescope). At least 10 measurements were performed on each surface.

2.2.4 Contact and Roll off Angle Measurements

The advancing contact angle, receding contact angle and roll off angle measurements of the testing liquid droplets were conducted using a Ramé-Hart 260-F4 goniometer. The advancing contact angles were measured by adding testing liquid continuously to the droplet of small volume of liquid (~8 μL) which ultimately forces the droplet to advance as shown in the Figure 2, whereas the receding contact angles were measured by removing the liquid from the droplet continuously which allows it to recede a shown in Figure 2.

The roll-off angles were measured by tilting the Ramé-Hart 260-F4 goniometer stage until the test liquid droplet rolled off from the surface. For each liquid, at least five measurements of advancing contact angles, receding contact angles and roll-off angles were performed on each surface. The contact angle and roll off angle measurement uncertainty was ±1º and ±0.5º, respectively.

2.2.5 Mechanical Durability

To assess the mechanical durability against liquids flowing past the surface, our superomniphobic surfaces were subjected to a shear stress of ~10 Pa using rotary flow in a beaker for ~1 hour. To assess the mechanical durability upon abrasion with solids, our superomniphobic surfaces were subjected to linear taber abrasion with a 1200 grit sandpaper under a shear stress of ~1 kPa.

2.2.6 Chemical Resistance

To assess the chemical resistance, our superomniphobic surfaces were immersed in corrosive (i.e., acidic and basic) liquids with a wide range of pH values ($1 < pH < 13$) for 1 hour.

2.3 Results and Discussion

2.3.1 Epilog Legend 36 Ext

This inexpensive, commercially available laser system is listed by the manufacturer as a continuous laser system, but our experiments have indicated that the laser system is quasi-continuous. A continuous wave laser emits a laser beam with a constant power, whereas, a pulsed laser emits pulses rather than one continuous beam. We have determined that the Epilog Legend 36 EXT is a quasi-continuous laser system by studying the variation of power with time. The experimental setup used to study the variation of power is shown in Figure 7. In this schematic (Figure 7a), the laser head is moving (speed = 20 mm/s) towards the +y direction and then comes back towards -y direction and this process repeats (over a 1" x 1" area). The beam is emitted toward -z (into the plane). The laser is reflected by a metal surface and the power is measured by a detector. The profile obtained (Figure 7b) indicates the time between adjacent peaks in power is on the order of milliseconds, which is much higher than a typical pulsed CO_2 laser system. So, we concluded that the laser system is quasi-continuous rather than continuous.

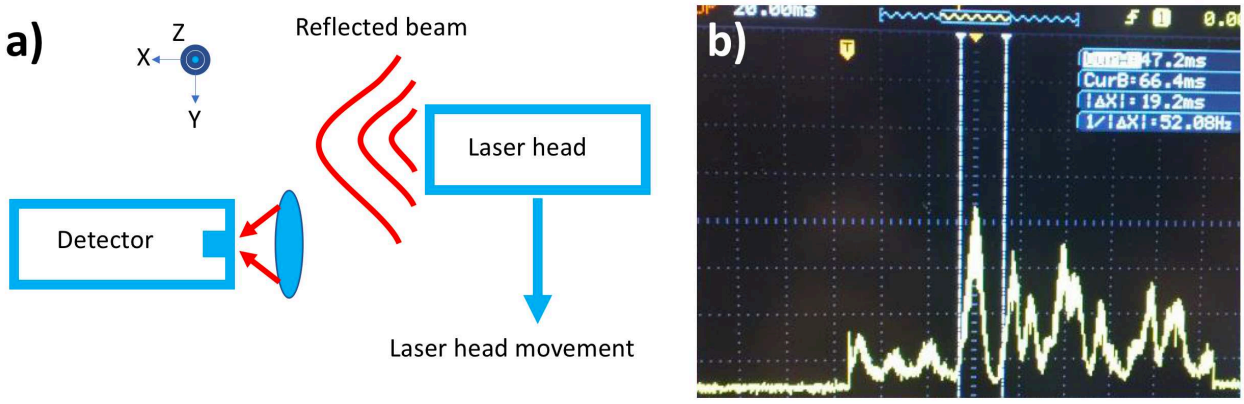

Figure 7: a) Schematic showing laser setup and movement. b) Oscilloscope image showing laser power as a function of time

2.4 Influence of Laser Power on Superomniphobicity of Surfaces

In this work, we fabricated nanostructured and re-entrant textured surfaces using the Epilog Legend 36 EXT with a central wavelength of 10.6 μm. Upon modifying the re-entrant textured surfaces with a fluorinated silane to impart low surface energy ($\gamma_{sv} \approx 10$ mN/m)[20,22,23] the surfaces displayed superomniphobicity towards liquids with surface tension $\geq$ 27.5 mN/m. The key parameters influencing the surface texture (and hence superomniphobicity) are the laser power and the laser raster speed[55-58]. In order to systematically investigate the influence of laser power on the surface texture and surface wettability, we ablated the surface of stainless steel 430 (a widely used industrial material) with different laser powers at a constant laser raster speed of 2 cm/s and subsequently modified the laser-ablated surfaces with a fluorinated silane. As received surfaces of stainless steel 430 displayed low surface roughness (R_{rms} = 0.53 μm, Figure 8a) and were omniphilic (θ^*_{adv} = 68°, θ^*_{rec} = 49° for water, γ_{lv} = 72.1 mN/m; and θ^*_{adv} = 38°, θ^*_{rec} = 16° for n-hexadecane, γ_{lv} = 27.5 mN/m). When the stainless steel 430 was subjected to laser ablation, the surface absorbed the laser energy, which resulted in a series of intertwined physical phenomena such as melting, vaporization, sublimation, splashing and re-solidification[40,55,56,59]. These complex laser-material interactions resulted in nanostructured (or rough) surfaces. As the laser power

increased, the surface roughness increased (see Figures 8a-8c) and resulted in enhanced liquid repellency (i.e., higher contact angles and lower roll off angles) after surface fluorination to impart low solid surface energy (Figures 8d-8e). For example, at an intermediate laser power of 84 W, a bump-like nanostructure with a feature size of ~50 nm (R_{rms} = 0.85 μm, Figure 8b) formed on the surface. Upon surface fluorination, the textured surface was omniphobic (θ^*_{adv} = 151°, θ^*_{rec} = 144°, ω = 13° for water and θ^*_{adv} = 136°, θ^*_{rec} = 122°, ω = 34° for n-hexadecane, Figure 8d and 8e). Apparent contact angles higher than the corresponding contact angles on fluorinated non-textured surfaces (θ_{adv} = 89°, θ_{rec} = 74° for water and θ_{adv} = 68°, θ_{rec} = 43° for n-hexadecane) and finite roll off angles for water and n-hexadecane indicate that both the liquid droplets have adopted the Cassie-Baxter state on this omniphobic surface. The apparent contact angles of n-hexadecane were lower than that of water due to its lower surface tension. As the laser power was increased further to 120 W (the maximum power of the CO_2 laser system employed in this work), a densely-packed bead-like nanostructure with a feature size of ~10 nm (R_{rms} = 1.43 μm, Figure 8c) formed on the surface. Upon surface fluorination, the surface was superomniphobic (θ^*_{adv} = 169°, θ^*_{rec} = 164°, ω = 1° for water and θ^*_{adv} = 167°, θ^*_{rec} = 161°, ω = 3° for n-hexadecane, Figure 8d and 8e) with droplets of water and n-hexadecane bouncing on the surface. The very high apparent contact angles and the very low roll off angles for water and n-hexadecane indicate that both the liquid droplets have adopted the Cassie-Baxter state on this superomniphobic surface.

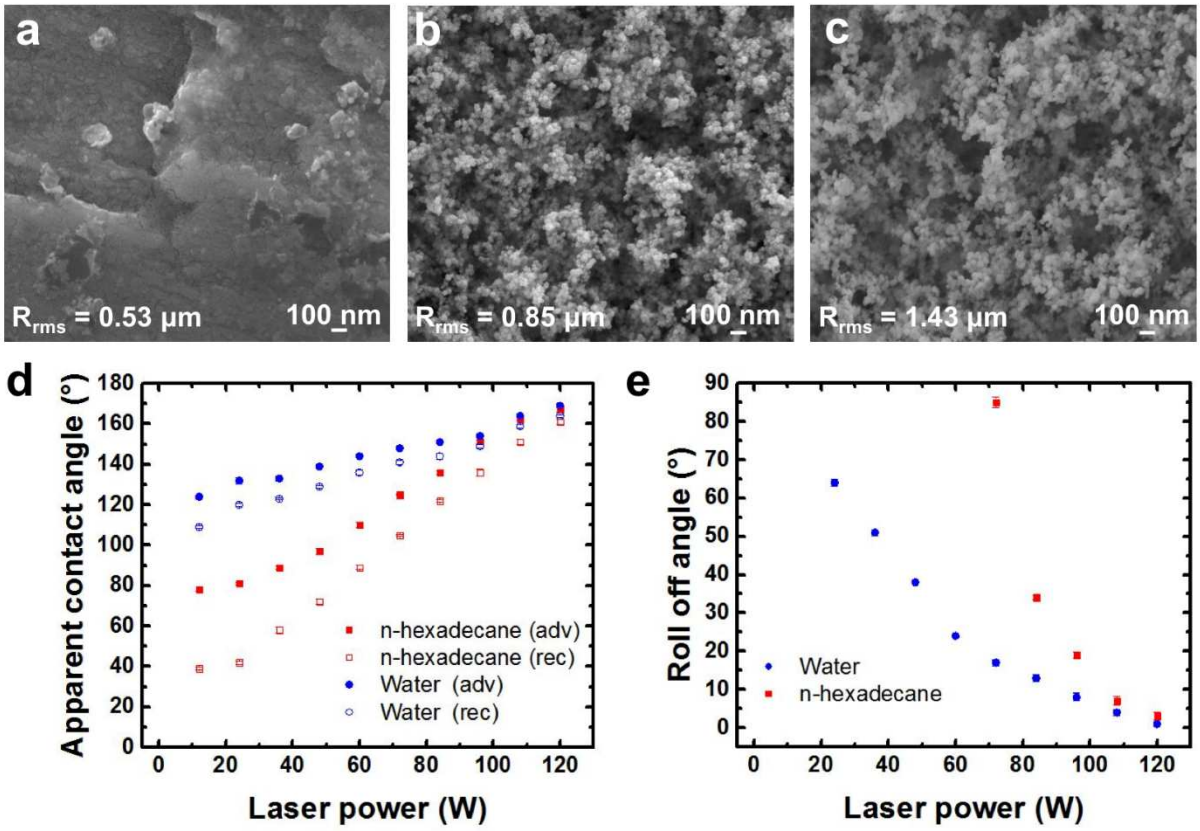

Figure 8: Scanning electron microscope (SEM) images showing the morphology of a) as-received stainless steel 430, b) surface textured at an intermediate laser power of 84 W, and c) surface textured at a high laser power of 120 W. d) and e) Apparent contact angles and roll off angles, respectively, of water and n-hexadecane droplets (~8 µL).

2.4.1 Influence of Laser Raster Speed on Superomniphobicity of Surfaces

In addition to laser power, the laser raster speed is another key parameter influencing the surface texture (and hence superomniphobicity)[55,56,60]. In order to systematically investigate the influence of laser raster speed on the surface texture and surface wettability, we ablated the surface of stainless steel 430 with different laser raster speeds at a constant laser power of 120 W and subsequently modified the laser-ablated surfaces with a fluorinated silane. As the laser raster speed decreased, the amount of laser energy absorbed by the surface per unit area increased[55,61], resulting in higher surface roughness (Figures 9a-9c) and consequently enhanced liquid repellency (i.e., higher contact angles and lower roll off angles) upon surface fluorination (Figures 9d and 9e). For example, at a high laser raster speed of 210 cm/s, the amount of laser energy absorbed by the

surface per unit area was insufficient to increase the surface roughness (R_{rms} = 0.58 μm, Figure 9a). Upon surface fluorination, the surface was omniphilic (θ^*_{adv} = 84°, θ^*_{rec} = 69° for water and θ^*_{adv} = 54°, θ^*_{rec} = 38° for n-hexadecane, Figure 9d and 9e). At an intermediate laser raster speed of 80 cm/s, a sparsely packed bead-like nanostructure with a feature size of ~30 nm (R_{rms} = 0.77 μm, Figure 9b) formed on the surface. Upon surface fluorination, the textured surface was omniphobic (θ^*_{adv} = 129°, θ^*_{rec} = 117°, ω = 70° for water and θ^*_{adv} = 73°, θ^*_{rec} = 54°, no roll off for n-hexadecane, Figure 9d and 9e). Apparent contact angles higher than the corresponding contact angles on fluorinated non-textured surfaces for water and finite roll off angles for water indicate that the water droplets adopted the Cassie-Baxter state on this omniphobic surface, while the no roll off for n-hexadecane indicates that it adopted the Wenzel state on this surface. At a low laser raster speed of 2 cm/s, the increased laser energy absorbed by the surface per unit area led to the formation of densely packed bead-like nanostructures with a feature size of ~10 nm (R_{rms} = 1.43 μm, Figure 9c). Upon surface fluorination, this surface was superomniphobic (θ^*_{adv} = 169°, θ^*_{rec} = 164°, ω = 1° for water and θ^*_{adv} = 167°, θ^*_{rec} = 161°, ω = 3° for n-hexadecane, Figure 9d and 9e).

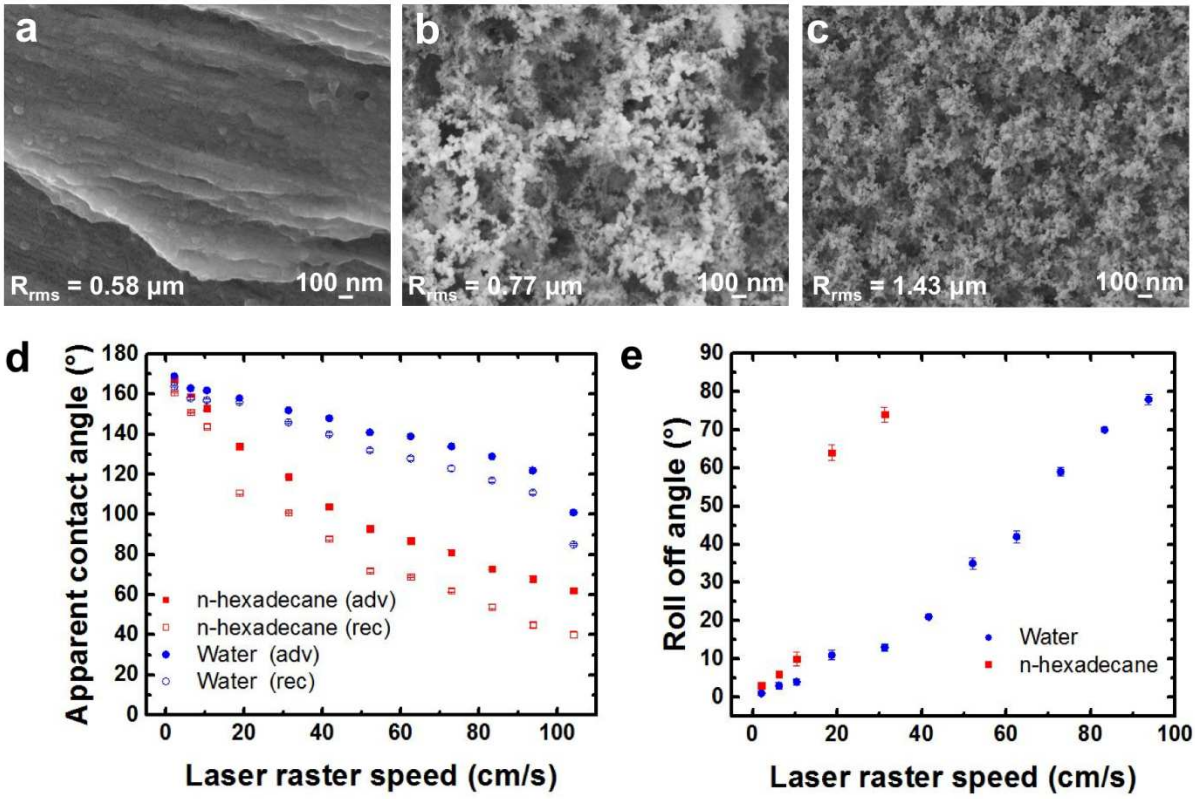

Figure 9: SEM images showing the morphology of stainless steel 430 surfaces textured at laser raster speeds of a) 210 cm/s, b) 80 cm/s, and c) 2 cm/s. d) and e) Apparent contact angles and roll off angles, respectively, of water and n-hexadecane droplets (~8 µL).

2.4.2 Fabrication of Omniphobic Surfaces with Different Materials

In a similar manner, we have tuned the laser parameters to determine the combination of laser power and laser raster speed that resulted in the maximum liquid repellency for a variety of materials. Utilizing our laser texturing technique, we fabricated superomniphobic surfaces with stainless steel 316 (θ^*_{adv} = 168°, θ^*_{rec} =164°, ω = 1° for water, and θ^*_{adv} = 162°, θ^*_{rec} =154°, ω = 4° for n-hexadecane), omniphobic surfaces with stainless steel 304 (θ^*_{adv} = 159°, θ^*_{rec} =153°, ω = 8° for water, and θ^*_{adv} = 116°, θ^*_{rec} =84°, ω = no roll off for n-hexadecane), omniphobic surfaces with titanium (θ^*_{adv} = 158°, θ^*_{rec} = 152°, ω = 7° for water and θ^*_{adv} = 112°, θ^*_{rec} = 92°, ω = no roll off for n-hexadecane), omniphobic surfaces with aluminum (θ^*_{adv} = 164°, θ^*_{rec} = 159°, ω = 5° for water

and θ^*_{adv} = 120°, θ^*_{rec} = 98°, ω = no roll off° for n-hexadecane), and omniphobic surfaces with glass (θ^*_{adv} = 161°, θ^*_{rec} = 156°, ω = 6° for water and θ^*_{adv} = 119°, θ^*_{rec} = 76°, ω = no roll off° for n-hexadecane) (see Table 2 and Figures 10a-10f). While all the surfaces were omniphobic (i.e., θ^* > 150° and ω < 10° with water), only the textured stainless steel 430 and 316 surfaces were superomniphobic (i.e., θ^* > 150° and ω < 10° with both water and n-hexadecane).

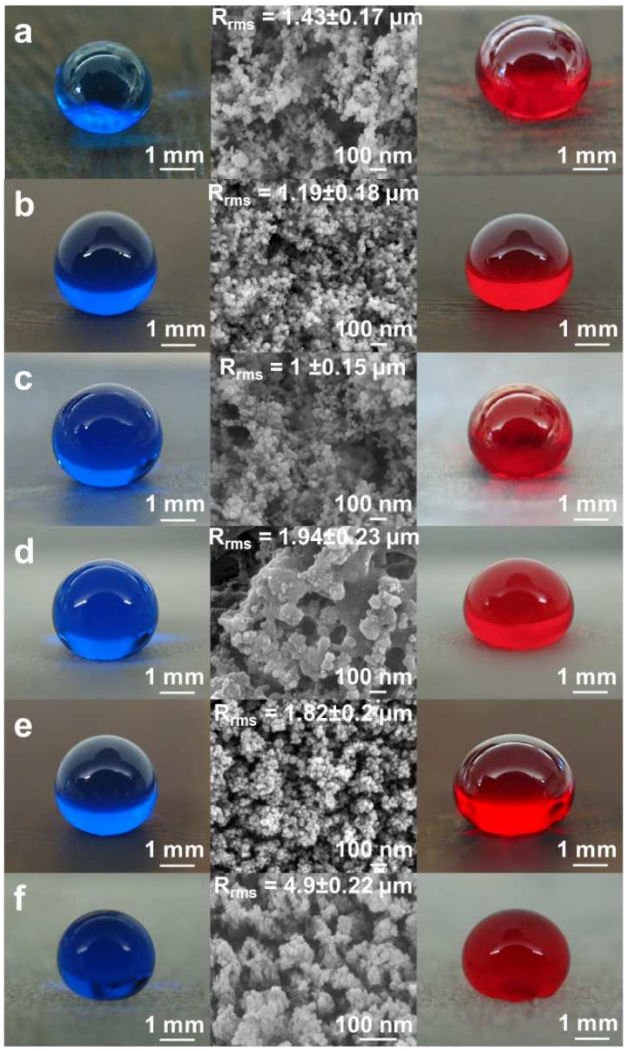

Figure 10: Images showing water droplets (dyed blue, on the left) and n-hexadecane droplets (dyed red, on the right) beading up on the laser textured and fluorinated (SEM images, in the middle) a) stainless steel 430, b) stainless steel 316, c) titanium, d) aluminum, e) stainless steel 304, and f) glass surfaces.

The different surface wettability obtained with different materials is due to the different surface textures induced by the complex laser-material interactions, which in turn depend on the material properties (e.g., melting point, thermal conductivity, reflectivity etc.) and the laser properties (e.g., laser focal spot size, temporal output profile etc.)[55,56,62,63].

2.4.3 X-ray Photoelectron Spectroscopy Results

Knowing that superomniphobicity is a strong function of surface chemistry, surface roughness, re-entrant texture and breakthrough pressure from prior extensive work[2,19,20,22,64,65], we have attempted to better identify (or eliminate) the possible parameters that are leading to the difference in wettability.

We conducted X-ray photo-electron spectroscopy (XPS) to assess the surface chemistry for all the laser ablated and silanized surfaces. We used XPS survey spectra (see Figure 11) to determine the ratio of fluorine (F) groups to carbon (C) groups and fluorine (F) groups to oxygen (O) groups (see Table 3). We anticipate that a higher F:C ratio or a higher F:O ratio will result is better liquid repellency. However, the results in Table 3 indicate that the F:C ratio and the F:O ratio cannot completely explain why stainless steel 430 and stainless steel 316 are superomniphobic, but the remaining materials are only omniphobic. In order to further characterize the surface chemical composition, we obtained the high-resolution C1s XPS spectra (see Figure 12) and the ratio of $–CF_3$ groups to the $–CF_2$ groups (which is a measure of the surface energy) for all the laser ablated and silanized surfaces (see Table 3). Although, the stainless steel 316, stainless steel 304 and titanium surfaces have similar ratios of $–CF_3$ groups to $–CF_2$ groups, only stainless steel 316 surfaces showed superomniphobicity. Also, the presence of metal carbonate groups (which are more philic) may explain the lack of superomniphobicity of stainless steel 304 and titanium surfaces (see Figure 12c and Figure 12d). However, such metal carbonate groups are absent on

aluminum surfaces and yet aluminum surfaces lack superomniphobicity, indicating that texture may be playing a role in addition to surface chemistry in determining whether or not a surface is superomniphobic.

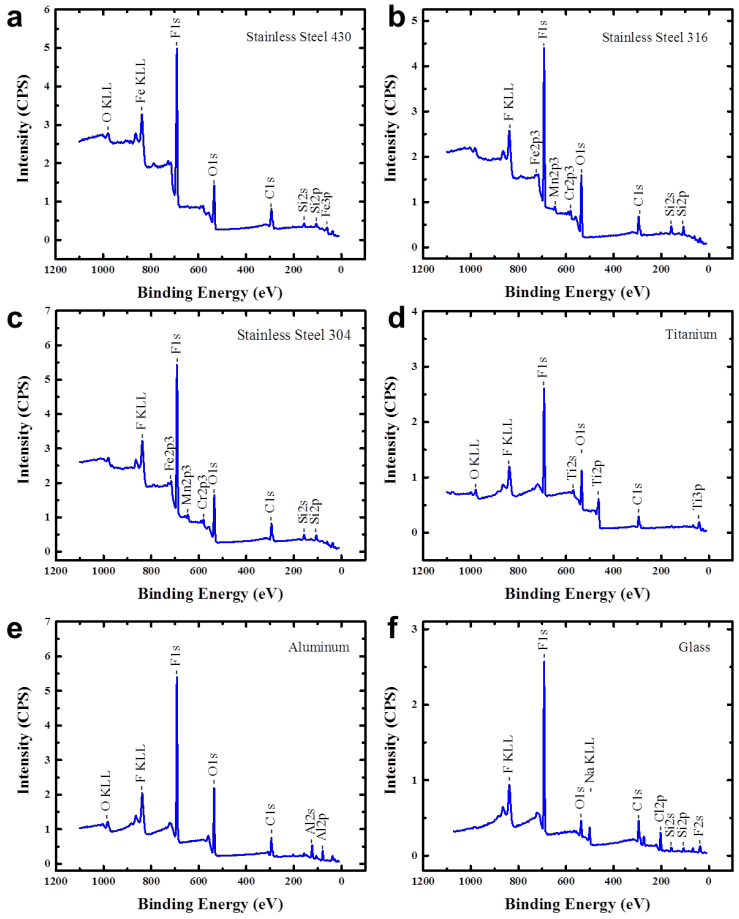

Figure 11: XPS survey spectra of laser ablated and silanized a) stainless steel 430, b) stainless steel 316, c) stainless steel 304, d) titanium, e) aluminum, and f) glass surfaces.

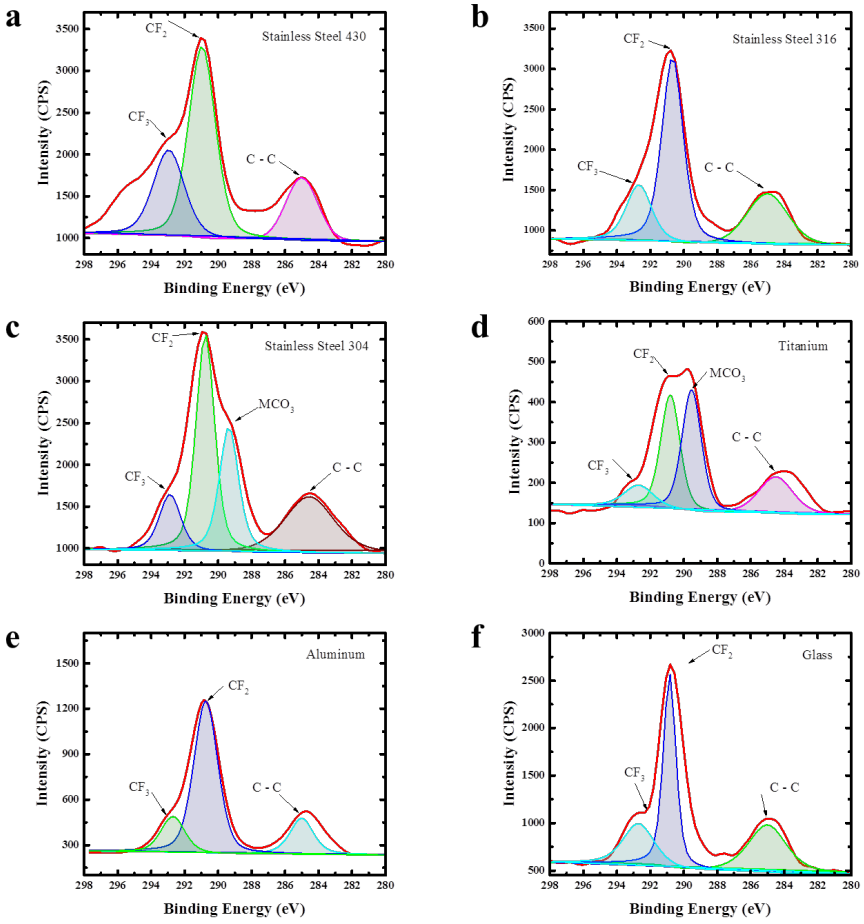

Figure 12: High-resolution C1s XPS spectra of laser ablated and silanized a) stainless steel 430, b) stainless steel 316, c) stainless steel 304, d) titanium, e) aluminum, and f) glass surfaces.

Table 2: Apparent advancing contact angles, apparent receding contact angles, roll off angles of water and n-hexadecane droplets on all our surfaces.

Substrate	Water			n-Hexadecane		
	θ_{adv} (°)	θ_{rec} (°)	ω (°)	θ_{adv} (°)	θ_{rec} (°)	ω (°)
SS 430	169	164	1	167	161	3
SS 316	168	164	1	162	154	4
SS 304	159	153	8	116	84	NR
Titanium	158	152	7	112	92	NR
Aluminum	164	159	5	120	98	NR
Glass	161	156	6	119	76	NR

Table 3: RMS roughness, F:O ratio, F:C ratio, and ratio of -CF_3 to -CF_2 groups of all our surfaces.

Substrate	RMS roughness (μm)	Ratio of Fluorine to Oxygen (F/O) groups	Ratio of Fluorine to Carbon (F/C) groups	Ratio of -CF_3 to -CF_2 groups
SS 430	1.43±0.17	3.5	6.1	0.6
SS 316	1.19±0.18	6.7	2.8	0.5
SS 304	1.82±0.20	3.3	6.5	0.5
Titanium	1.00±0.15	2.4	9.1	0.5
Aluminum	1.94±0.23	2.4	7.8	0.4
Glass	4.90±0.22	5.9	5.9	0.4

We also conducted RMS roughness measurements for all the laser ablated and silanized surfaces to assess the surface roughness (see Table 3). Our RMS roughness measurements for all the metal and metal alloy surfaces are not significantly different from each other. The RMS roughness of the glass surfaces is slightly higher, and yet glass surfaces do not display superomniphobicity. Consequently, we infer that surface roughness is not the primary factor leading to the differences in wettability. Having eliminated the surface roughness as the primary factor, we speculate that the difference in wettability arises from (i) high inter-feature spacing, leading to low breakthrough pressure [64,65] locally on the surface, and/or (ii) lack of re-entrant texture locally on the surface, and/or (iii) surface chemistry.

2.4.4 Re-Entrant Texture and Inter Feature Spacing

On the surfaces that are only omniphobic and not superomniphobic (i.e., stainless steel 304, titanium, aluminum and glass), we believe that the n-hexadecane droplets have adopted a hybrid wetting state with partial Cassie-Baxter state and partial Wenzel state. In other words, for the surfaces that are omniphobic, but not superomniphobic (i.e., stainless steel 304, titanium,

aluminum and glass), we believe that there are local areas that do not possess enough re-entrant texture and/or there are local areas with high inter-feature spacing (leading to low breakthrough pressure). Figure 13 shows the SEM images of stainless steel 304, titanium, aluminum and glass with a wide range of inter-feature spacing 2D (shown by red lines) and areas without re-entrant texture (shown with regions enclosed by yellow lines).

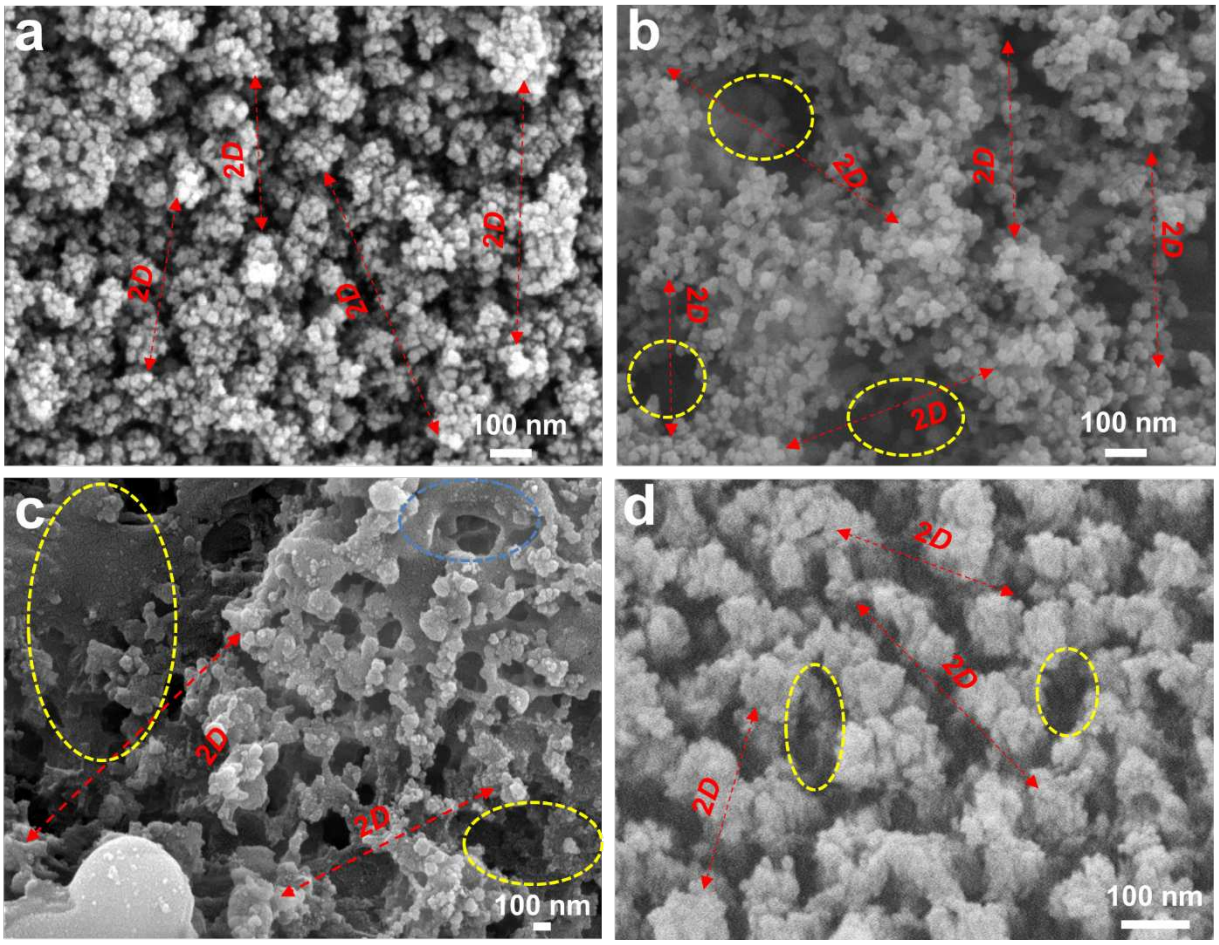

Figure 13: Scanning electron microscope (SEM) images showing the morphology of laser textured a) stainless steel 304, b) titanium, c) aluminum, and d) glass surfaces. The red lines indicate a wide range of inter-feature spacing 2D. The regions enclosed by the yellow lines indicate areas without re-entrant texture.

2.4.5 Chemical and Mechanical Resistance

Further, we assessed the chemical resistance of our superomniphobic surfaces. Our surfaces retained their superomniphobicity (i.e., no change in apparent contact angles or roll off angles for water and n-hexadecane) when immersed in corrosive (i.e., acidic and basic) liquids with a wide pH range. We also assessed the mechanical durability of our superomniphobic surfaces. While our surfaces retained their superomniphobicity (i.e., no change in apparent contact angles or roll off angles for water and n-hexadecane) against liquids flowing past the surface for a short time, they immediately lost their superomniphobicity upon abrasion with solids.

2.4.6 Applications

Our laser texturing technique enables simple, inexpensive, scalable and solvent-free fabrication of nanostructured surfaces with patterned wettability on a wide range of materials via selective laser ablation. In order to demonstrate this, we fabricated patterned surfaces ("CSU" pattern as an example) with significant wettability contrast on glass by texturing a glass surface everywhere except the "CSU" pattern. Upon fluorination, the textured surface was superhydrophobic and the non-textured surface (i.e., "CSU" pattern) was hydrophobic. When water droplets (dyed blue) were deposited everywhere on this patterned surface, they selectively adhered to the hydrophobic surface and rolled off easily from the superhydrophobic surface to result in a "CSU" liquid pattern (Figure 14a). In addition, our laser texturing technique also allows easy fabrication of a single nanostructured surface with discrete domains of the desired wettability by tuning the surface texture. To illustrate this, we fabricated a titanium surface with multiple, discrete domains with different surface textures by using the same laser power, but different laser raster speeds (Figure 14b). Upon fluorination, as anticipated, each discrete domain displayed different wettability (Figure 14c-14f) due to the different surface texture. Further, our laser texturing technique can be

used to fabricate on-surface microfluidic devices with a wide variety of patterns. To illustrate this, we fabricated a circular guiding track by laser texturing a stainless steel 430 surface everywhere except the circular track. Upon fluorination, the textured surface was superhydrophobic and the non-textured surface (i.e., the circular track) was hydrophobic. When a water droplet was placed on the circular track, it was confined to the hydrophobic track due to the wettability contrast induced by the surrounding superhydrophobic surface. As the surface was tilted, when the work done by gravity overcame the work expended due to adhesion between water and the hydrophobic surface, the water droplet moved along the circular track (Figure 14g-14f).

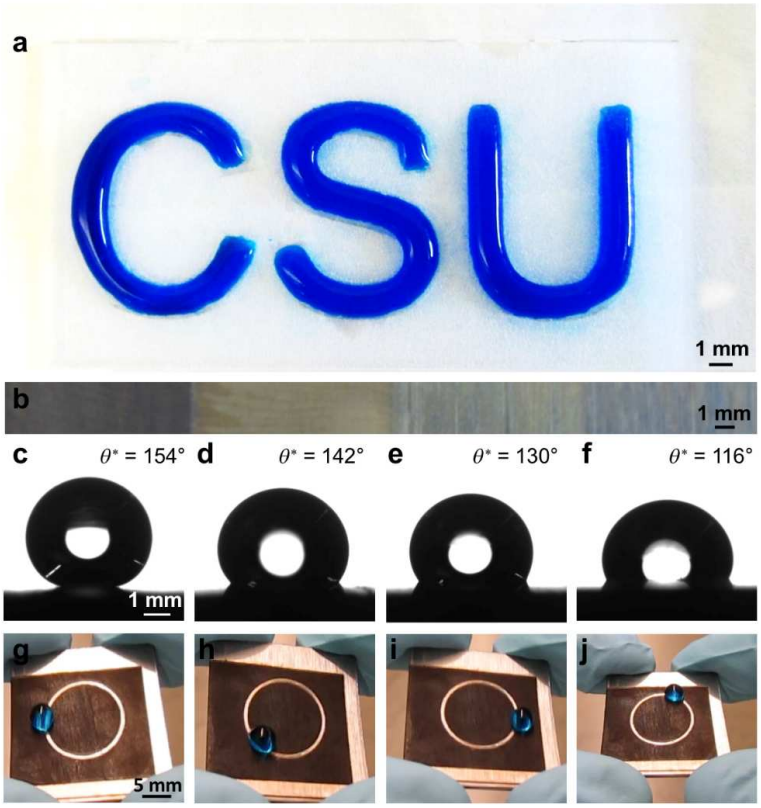

Figure 14:a) Image illustrating the "CSU" liquid pattern (with water, dyed blue) on the textured glass surface with wettability contrast. b) A titanium surface with four discrete domains with different surface textures obtained by using the same laser power, but different laser raster speeds. c), d), e) and f) Water droplets on the four discrete domains with different wettability. g), h), i) and j) Series of images showing water droplet (dyed blue) moving along the circular guiding tracking on a stainless steel 430 surface

3 FABRICATION OF SUPEROMNIPHOBIC GLASS MICROFIBER PAPER WITH SILICONE NANOFILAMENTS

3.1 Background

Fabrication of superomniphobic surfaces using cellulose-based paper and other inexpensive materials like cellulose filter paper, cotton balls, cellulose cloth, glass microfiber insulation, glass microfiber filter paper is gaining importance due to its flexible and economical usage in manufacturing of microfluidic devices for numerous modern world applications. In some of the reported works in literature[66], the droplets of low surface tension liquid often have high contact angles (CA>150°) but adhere on the surface and cannot roll off, even when the surface is turned upside down. The adhesion between droplets of low surface tension liquids and superomniphobic surfaces should be very low which will allow the droplet to roll off easily (roll off angle< 10°). In order to fabricate these superomniphobic surfaces, creating appropriate surface micro/nanostructure and lowering overall surface energy of the substrate can be considered as two important phases. There are only a few studies that have reported such low roll off angles (<10°) for low surface tension liquids by using inherently textured inexpensive surfaces as substrates or by introducing some specially designed patterns, such as overhang structures and re-entrant surface curvatures mostly on silicon wafers and aluminum foil substrates. Therefore, we present a simple approach for the fabrication of superomniphobic glass microfiber paper surfaces by the combination of creating micro/nano textured silicone nanofilaments.

3.2 Materials/Methods/Experiments

3.2.1 Fabrication of Superomniphobic Glass Microfiber Paper

Prior to fabrication of silicone nanofilaments, glass microfiber paper (Figure 15b) samples were cleaned by sonication in acetone and ethanol, dried with nitrogen and treated with O_2 plasma. The surfaces were exposed to water vapor for 2 minutes prior to the treatment. In controlled humid conditions, silicone nanofilaments with different micro and nanostructures were grown in toluene onto glass slides by hydrolysis and condensation of trichloromethylsilane (TCMS).

Under atmospheric humid conditions, 400 mL of toluene was thoroughly mixed with 3μL of water of shaker for 10 minutes. 250 μL of trichloromethylsilane (TCMS) was added to the mixture of toluene and water and shaken for 10 minutes. The samples were immersed in the final solution of toluene, DI water and trichloromethylsilane (TCMS). Under controlled humid conditions (>60% Relative Humidity), this whole system was left idle for 6 hours. These treated samples were annealed in an oven at 300°F for 4 hours. The final samples were rinsed with toluene, ethanol and of 50% v/v DI water/ethanol solution successively, and were dried under a nitrogen flow.

Subsequently, the nanofilaments were activated using O_2 plasma and then modified with heptadecafluoro-1,1,2,2-tetrahydrodecyl trichlorosilane (Gelest) via vapor phase silanization to reduce the overall surface energy of these glass microfiber paper surfaces. The superomniphobic glass microfiber paper surfaces (Figure 15c) thus obtained feature a high apparent contact angles ($\theta^* > 150°$) and ultralow pre-tilt angles ($\omega < 10°$) for low surface tension liquids like n-hexadecane.

3.2.2 Vapor Phase Silanization

The textured glass microfiber surfaces were subsequently modified via vapor phase silanization at 120°C for 1 hour using 200 μL of heptadecafluoro-1,1,2,2-tetrahydrodecyl trichlorosilane (Gelest) to impart low solid surface energy ($\gamma_{sv} \approx 10$ mN/m).

3.2.3 Characterization of Surface Morphology and Surface Roughness

The surfaces were imaged using a scanning electron microscope (JEOL JSM-6500F) at 15 kV to determine the surface morphology.

3.2.4 Contact and Roll off Angle Measurements

The advancing contact angle, receding contact angle and roll off angle measurements of the testing liquid droplets were conducted using a Ramé-Hart 260-F4 goniometer. The advancing contact angles were measured by adding testing liquid continuously to the droplet of small volume of liquid (~8 μL) which ultimately forces the droplet to advance as shown in the Figure 2, whereas the receding contact angles were measured by removing the liquid from the droplet continuously which allows it to recede a shown in Figure 2.

The roll-off angles were measured by tilting the Ramé-Hart 260-F4 goniometer stage until the test liquid droplet rolled off from the surface. For each liquid, at least five measurements of advancing contact angles, receding contact angles and roll-off angles were performed on each surface. The contact angle and roll off angle measurement uncertainty was ±1º and ±0.5º, respectively.

3.2.5 Chemical Resistance

To assess the chemical resistance, our superomniphobic glass microfiber paper surfaces were immersed in corrosive (i.e., acidic and basic) liquids with a wide range of pH values ($1 < pH < 13$).

3.3 Results

In this work, we fabricated silicone nanofilaments on glass microfiber paper (Figure 15b) surfaces by hydrolysis and condensation of trichloromethylsilane (TCMS) under controlled humid conditions. Upon modifying these textured surfaces with a fluorinated silane which impart low

surface energy ($\gamma_{sv} \approx 10$ mN/m), these surfaces (Figure 15c) displayed superomniphobicity towards liquids with surface tension ≥ 27.5 mN/m (Figure 15a).

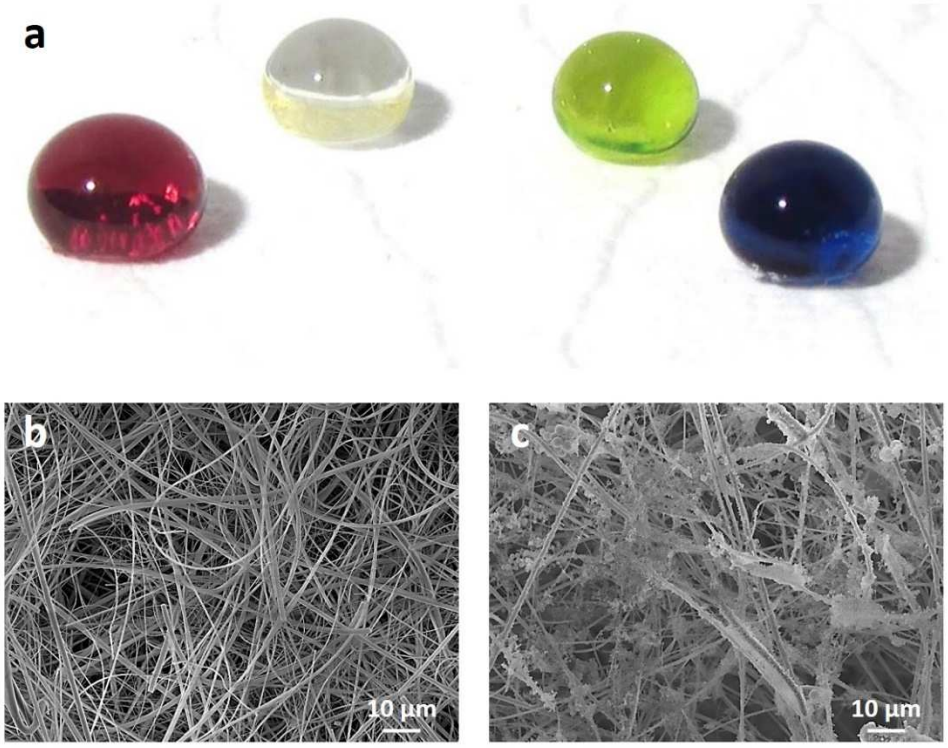

Figure 15: a) Droplets of Hexadecane (Red, γlv = 27.5 mN m^{-1}), Rapeseed oil (colorless, γlv = 35.7 mN m^{-1}), Glycerol (Green, γlv = 64 mN m^{-1}) and Water (Blue, γlv = 72.1 mN m^{-1}) beading up on superomniphobic glass microfiber paper. b) Scanning Electron Microscopic image of untreated Glass microfiber paper surface. c) Scanning Electron Microscopic image of superomniphobic glass microfiber paper surface.

3.4 Applications

3.4.1 Stable and Flexible Superomniphobic Surfaces

Superomniphobic glass microfiber paper surfaces can be used as stable platforms for enhanced floating in liquids with a wide range of surface tensions. Recent work has indicated that flexible surfaces on a liquid have higher weight bearing capacity and better floating stability compared to rigid sheets of similar thickness and lateral dimensions.[22] Here, the weight-bearing capacity is the maximum weight that the film can support before sinking. In order to evaluate the weight bearing capacity of our superomniphobic glass microfiber paper surfaces, we have placed them on water

and rapeseed oil (Figure 16). These surfaces were subjected to gradually increasing force using circular force probes until the surfaces were completely submerged in testing liquid. Force was measured with a force gauge (±0.5 mN resolution). Our surfaces can withstand a weight of 47 mN and 34 mN on water and rapeseed oil respectively. The stability of these superomniphobic glass microfiber paper surfaces will encourage the use of these surfaces to fabricate stages for micro robots for numerous applications on oil spills and contaminated aqueous media.

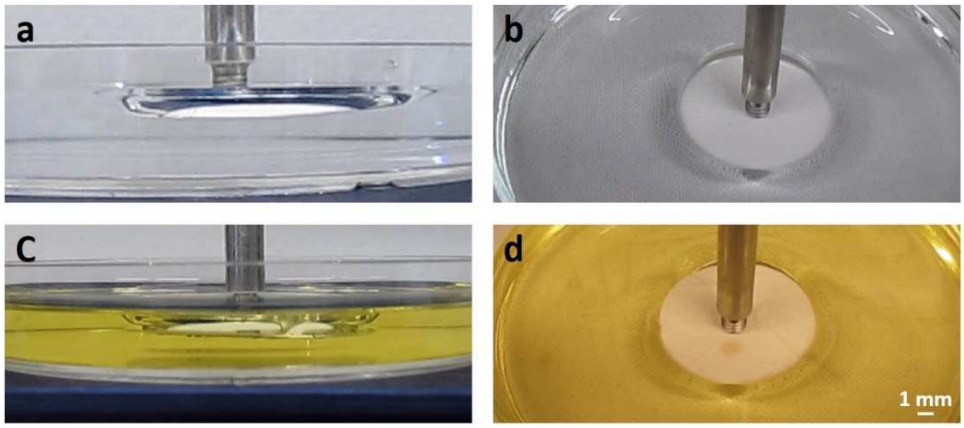

Figure 16: a), b) showing the weight bearing capacity of superomniphobic glass microfiber paper surface on water (γlv = 72.1 mN m^{-1}). c), d) showing the weight bearing capacity of superomniphobic glass microfiber paper surface on rapeseed oil (γlv = 35.7 mN m^{-1}).

3.4.2 Marangoni Convention

These superomniphobic glass microfiber paper surfaces can be used as self-propelled striders. The mobility of these surfaces can be controlled by the Marangoni effect. Whenever a surface tension gradient arises in a fluid, the fluid molecules move from the regions of higher surface tension to regions of lower surface tension; this is called is called Marangoni effect[67]. Our Marangoni effect propelled strider can be moved on a propylene glycol (γ_{LV} = 45.6 mN/m) bath using acetone (γ_{LV} = 25.2 mN/m) as driving fuel (Figure 17). Acetone was released from a pipette into the propylene glycol. When acetone was mixed with propylene glycol only on one side of the strider, a surface tension gradient was generated across the strider. As a result, a net force was generated from the

surface tension gradient, which propelled the strider. The propulsion of these striders could be tuned for either continuous or intermittent motion, by changing the way the acetone was mixed with the propylene glycol.

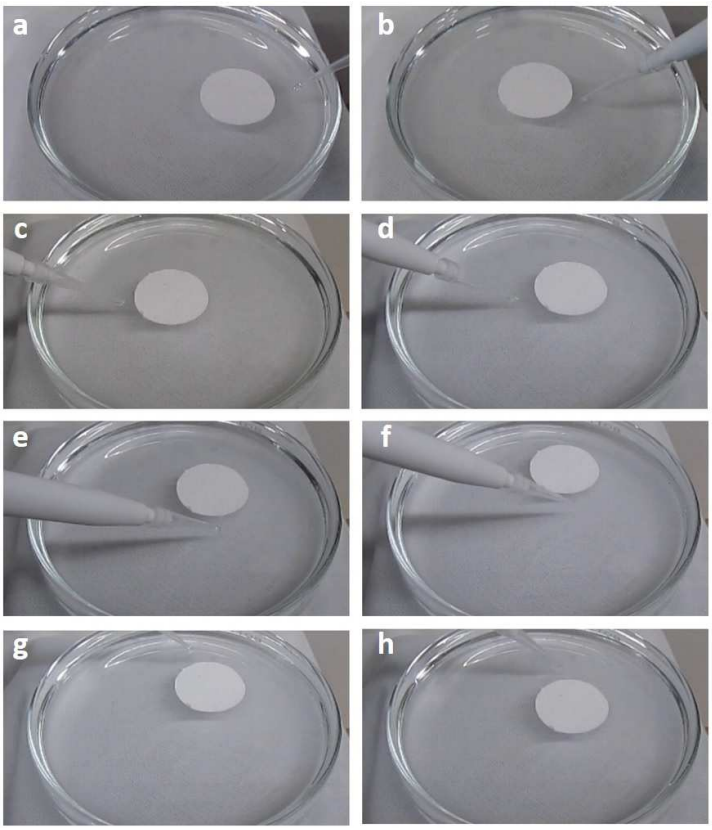

Figure 17: a), b) Images showing the motion of superomniphobic glass microfiber paper surface in negative X-direction. c), d) Images showing the motion of superomniphobic glass microfiber paper surface in positive X-direction. e), f) Images showing the motion of superomniphobic glass microfiber paper surface in positive Y-direction. g), h) Images showing the motion of superomniphobic glass microfiber paper surface in negative Y-direction.

3.4.3 Chemical Shielding

We assessed the chemical resistance of our superomniphobic glass microfiber paper surfaces by testing them under corrosive environments for 12 hours. Our surfaces retained their superomniphobicity (i.e., no change in apparent contact angles or pre-tilt off angles of hexadecane) when immersed in corrosive (i.e., acidic and basic) liquids with a wide pH range of 4 to 11 (Figure 18).

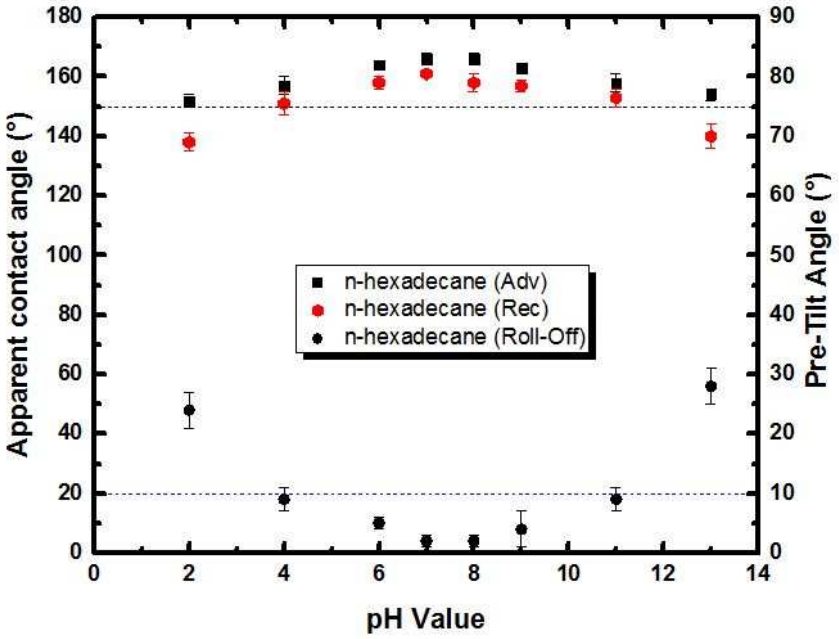

Figure 18: Variation in contact angles with the change in pH value of environment after 12 hours.

4 CONCLUSION

4.1 Fabrication of Nanostructured Omniphobic and Superomniphobic Surfaces with Inexpensive CO_2 Laser Engraver

We demonstrated the fabrication of nanostructured omniphobic and superomniphobic surfaces with a wide variety of materials using a simple, inexpensive, scalable and solvent-free CO_2 laser texturing technique. In order to obtain the appropriate surface texture necessary for maximum liquid repellency, we investigated the influence of laser power and laser raster speed on the surface texture and surface wettability. Our laser texturing technique can be used to fabricate patterned surfaces, surfaces with discrete domains of the desired wettability and on-surface microfluidic devices.

4.2 Fabrication of Superomniphobic Glass Microfiber Paper with Silicone Nanofilaments

In this preliminary work, we have demonstrated a simple method to fabricate superomniphobic glass microfiber paper surfaces. These surfaces can withstand a weight of 47 mN and 34 mN on water and rapeseed oil respectively. We also engineered striders with highly controlled locomotion, using Marangoni Convention. Overall, the strider's ability to float freely and execute precisely controlled locomotion, even on low surface tension liquids like propylene glycol, makes it a promising new platform for numerous applications on oil spills or contaminated aqueous media.

5 FUTURE WORK

5.1 Fabrication of Nanostructured Omniphobic and Superomniphobic Surfaces with Inexpensive CO_2 Laser Engraver

In this work, we presented a solution to fabricate superomniphobic stainless steel surfaces using a simple, inexpensive, scalable and solvent-free laser texturing technique which subsequently favors fabrication of gradient wettability surfaces, and droplet manipulation tracks with a wide variety of materials. This current laser texturing technique works well for small-scale applications and testing. However, these superomniphobic surfaces are not durable, exposure to harsh mechanical environments tends to degrade the superomniphobicity of these surfaces significantly. The degradation of these superomniphobic surfaces is mainly due to the liberally attached nanostructured particles formed during the continuous melting and re-solidification process during laser ablation. In order to demonstrate practical applications, there is a need for proper heat treatment to be done to firmly attach the particles to the substrate in order to preserve the superomniphobicity.

Future work should also investigate laser texturing techniques to fabricate superomniphobic surfaces in a cost-effective manner by reducing processing times by an order of magnitude. Laser material interactions, being a complex subject must be studied in further detail to evolve many sophisticated ways to fabricate superomniphobic surfaces with a wide variety of substrates.

5.2 Fabrication of Superomniphobic Glass Microfiber Paper with Silicone Nanofilaments

In this work, we have presented a simple method to fabricate the superomniphobic glass microfiber paper surfaces. However, the durability of these surfaces is the main concern to be able to use them for practical purposes. In future, the necessary steps to increase the durability of these

superomniphobic surfaces must be investigated. There is a need to investigate new methods to fabricate these flexible superomniphobic surfaces in a more economical way by reducing the time of fabrication further.

These superomniphobic surfaces can be used to fabricate portable and cost effective microfluidic devices that can handle liquids with a wide range of surface tensions. These superomniphobic surfaces combined with appropriate geometrical design can be used as load carrying vehicles on aqueous solution. These superomniphobic surfaces can be self-propelled by having a fuel tank of lower surface tension liquid that constantly adds the driving drop by drop to create difference in surface tension which initiates Marangoni effect.

REFERENCES

1 Butt, H. J. *et al.* Characterization of super liquid-repellent surfaces. *Current Opinion in Colloid & Interface Science* **19**, 343-354, doi:10.1016/j.cocis.2014.04.009 (2014).

2 Kota, A. K., Kwon, G. & Tuteja, A. The design and applications of superomniphobic surfaces. *NPG Asia Materials* **6**, e109 (2014).

3 Xi, J. & Jiang, L. Biomimic superhydrophobic surface with high adhesive forces. *Industrial & Engineering Chemistry Research* **47**, 6354-6357, doi:10.1021/ie071603n (2008).

4 Xia, F. & Jiang, L. Bio-inspired, smart, multiscale interfacial materials. *Advanced Materials* **20**, 2842-2858, doi:10.1002/adma.200800836 (2008).

5 Jin, M. H. *et al.* Superhydrophobic aligned polystyrene nanotube films with high adhesive force. *Advanced Materials* **17**, 1977-+, doi:10.1002/adma.200401726 (2005).

6 Jiang, T., Guo, Z. G. & Liu, W. M. Biomimetic superoleophobic surfaces: focusing on their fabrication and applications. *J. Mater. Chem. A* **3**, 1811-1827, doi:10.1039/c4ta05582a (2015).

7 Patankar, N. A. Mimicking the lotus effect: influence of double roughness structures and slender pillars. *Langmuir* **20**, 8209-8213, doi:10.1021/la048629t (2004).

8 Barthlott, W. & Neinhuis, C. Purity of the sacred lotus, or escape from contamination in biological surfaces. *Planta* **202**, 1-8, doi:10.1007/s004250050096 (1997).

9 Youngblood, J. P., Sottos, N. R. & Extrand, C. Bioinspired materials or self-cleaning and self-healing. *Mrs Bulletin* **33**, 732-741, doi:10.1557/mrs2008.158 (2008).

10 Bhushan, B. & Jung, Y. C. Natural and biomimetic artificial surfaces for superhydrophobicity, self-cleaning, low adhesion, and drag reduction. *Progress in Materials Science* **56**, 1-108, doi:10.1016/j.pmatsci.2010.04.003 (2011).

11 Bittoun, E. & Marmur, A. The Role of Multiscale Roughness in the Lotus Effect: Is It Essential for Super-Hydrophobicity? *Langmuir* **28**, 13933-13942, doi:10.1021/la3029512 (2012).

12 Gao, L. C. & McCarthy, T. J. The "lotus effect" explained: Two reasons why two length scales of topography are important. *Langmuir* **22**, 2966-2967, doi:10.1021/la0532149 (2006).

13 Su, Y. *et al.* Nano to Micro Structural Hierarchy Is Crucial for Stable Superhydrophobic and Water-Repellent Surfaces. *Langmuir* **26**, 4984-4989, doi:10.1021/la9036452 (2010).

14 Bonn, D., Eggers, J., Indekeu, J., Meunier, J. & Rolley, E. Wetting and spreading. *Reviews of Modern Physics* **81**, 739-805, doi:10.1103/RevModPhys.81.739 (2009).

15 Chaudhury, M. K. & Whitesides, G. M. HOW TO MAKE WATER RUN UPHILL. *Science* **256**, 1539-1541, doi:10.1126/science.256.5063.1539 (1992).

16 Wenzel, R. N. Resistance of solid surfaces to wetting by water. *Industrial & Engineering Chemistry* **28**, 988-994 (1936).

17 Nishimoto, S. & Bhushan, B. Bioinspired self-cleaning surfaces with superhydrophobicity, superoleophobicity, and superhydrophilicity. *Rsc Advances* **3**, 671-690 (2013).

18 Liu, K., Tian, Y. & Jiang, L. Bio-inspired superoleophobic and smart materials: Design, fabrication, and application. *Progress in Materials Science* **58**, 503-564, doi:10.1016/j.pmatsci.2012.11.001 (2013).

19 Tuteja, A. *et al.* Designing superoleophobic surfaces. *Science* **318**, 1618-1622 (2007).

20 Movafaghi, S. *et al.* Tunable superomniphobic surfaces for sorting droplets by surface tension. *Lab on a Chip* **16**, 3204-3209 (2016).
21 Wang, W. *et al.* Superhydrophobic coatings with edible materials. *ACS applied materials & interfaces* **8**, 18664-18668 (2016).
22 Vahabi, H., Wang, W., Movafaghi, S. & Kota, A. K. Free-standing, flexible, superomniphobic films. *ACS applied materials & interfaces* **8**, 21962-21967 (2016).
23 Movafaghi, S. *et al.* Hemocompatibility of Superhemophobic Titania Surfaces. *Advanced Healthcare Materials* (2016).
24 Bartlet, K., Movafaghi, S., Kota, A. & Popat, K. C. Superhemophobic titania nanotube array surfaces for blood contacting medical devices. *RSC Advances* **7**, 35466-35476 (2017).
25 Bark, D. L. *et al.* Hemodynamic performance and thrombogenic properties of a superhydrophobic Bileaflet mechanical heart valve. *Annals of biomedical engineering* **45**, 452-463 (2017).
26 Wang, W. *et al.* Metamorphic Superomniphobic Surfaces. *Advanced Materials* (2017).
27 Vahabi, H. *et al.* Metallic superhydrophobic surfaces via thermal sensitization. *Applied Physics Letters* **110**, 251602 (2017).
28 Vahabi, H., Wang, W., Davies, S., Mabry, J. M. & Kota, A. K. Coalescence-Induced Self-Propulsion of Droplets on Superomniphobic Surfaces. *ACS Applied Materials & Interfaces* **9**, 29328-29336 (2017).
29 Erbil, H. Y., Demirel, A. L., Avcı, Y. & Mert, O. Transformation of a simple plastic into a superhydrophobic surface. *Science* **299**, 1377-1380 (2003).
30 Lafuma, A. & Quéré, D. Superhydrophobic states. *Nature materials* **2**, 457-460 (2003).
31 Liu, M., Wang, S., Wei, Z., Song, Y. & Jiang, L. Bioinspired design of a superoleophobic and low adhesive water/solid interface. *Advanced Materials* **21**, 665-669 (2009).
32 Liu, T. & Kim, C. Turning a surface superrepellent even to completely wetting liquids. *Science* **346**, 1096-1100 (2014).
33 Kota, A. K., Mabry, J. M. & Tuteja, A. Superoleophobic surfaces: design criteria and recent studies. *Surface Innovations* **1**, 71-83 (2013).
34 Chu, Z. & Seeger, S. Superamphiphobic surfaces. *Chemical Society Reviews* **43**, 2784-2798 (2014).
35 Deng, X., Mammen, L., Butt, H.-J. & Vollmer, D. Candle soot as a template for a transparent robust superamphiphobic coating. *Science* **335**, 67-70 (2012).
36 Gao, L. & McCarthy, T. J. The "lotus effect" explained: two reasons why two length scales of topography are important. *Langmuir* **22**, 2966-2967 (2006).
37 Herminghaus, S. Roughness-induced non-wetting. *EPL (Europhysics Letters)* **52**, 165 (2000).
38 Baldacchini, T., Carey, J. E., Zhou, M. & Mazur, E. Superhydrophobic surfaces prepared by microstructuring of silicon using a femtosecond laser. *Langmuir* **22**, 4917-4919 (2006).
39 Kietzig, A.-M., Hatzikiriakos, S. G. & Englezos, P. Patterned superhydrophobic metallic surfaces. *Langmuir* **25**, 4821-4827 (2009).
40 Wu, B. *et al.* Superhydrophobic surfaces fabricated by microstructuring of stainless steel using a femtosecond laser. *Applied Surface Science* **256**, 61-66 (2009).
41 Chen, F. *et al.* Anisotropic wetting on microstrips surface fabricated by femtosecond laser. *Langmuir* **27**, 359-365 (2010).

42 Jagdheesh, R., Pathiraj, B., Karatay, E., Romer, G. & Huis in ‘t Veld, A. Laser-induced nanoscale superhydrophobic structures on metal surfaces. *Langmuir* **27**, 8464-8469 (2011).
43 Chen, F. *et al.* Bioinspired wetting surface via laser microfabrication. *ACS applied materials & interfaces* **5**, 6777-6792 (2013).
44 Moradi, S., Kamal, S., Englezos, P. & Hatzikiriakos, S. G. Femtosecond laser irradiation of metallic surfaces: effects of laser parameters on superhydrophobicity. *Nanotechnology* **24**, 415302 (2013).
45 Ta, D. V. *et al.* Nanosecond laser textured superhydrophobic metallic surfaces and their chemical sensing applications. *Applied Surface Science* **357**, 248-254 (2015).
46 Ahmmed, K. T. & Kietzig, A.-M. Drag reduction on laser-patterned hierarchical superhydrophobic surfaces. *Soft matter* **12**, 4912-4922 (2016).
47 Dunn, A. *et al.* Laser textured superhydrophobic surfaces and their applications for homogeneous spot deposition. *Applied Surface Science* **365**, 153-159 (2016).
48 Li, B.-j., Li, H., Huang, L.-j., Ren, N.-f. & Kong, X. Femtosecond pulsed laser textured titanium surfaces with stable superhydrophilicity and superhydrophobicity. *Applied Surface Science* **389**, 585-593 (2016).
49 Vorobyev, A. & Guo, C. Multifunctional surfaces produced by femtosecond laser pulses. *Journal of Applied Physics* **117**, 033103 (2015).
50 Groenendijk, M. Fabrication of super hydrophobic surfaces by fs laser pulses. *Laser Technik Journal* **5**, 44-47 (2008).
51 Yong, J. *et al.* Femtosecond laser ablated durable superhydrophobic PTFE films with micro-through-holes for oil/water separation: Separating oil from water and corrosive solutions. *Applied Surface Science* **389**, 1148-1155 (2016).
52 Fan, W. *et al.* A facile method to fabricate superamphiphobic polytetrafluoroethylene surface by femtosecond laser pulses. *Chemical Physics Letters* **644**, 261-266 (2016).
53 Li, H. *et al.* Multifunctional wettability patterns prepared by laser processing on superhydrophobic TiO 2 nanostructured surfaces. *Journal of Materials Chemistry B* **3**, 342-347 (2015).
54 Zhang, D. *et al.* A simple way to achieve pattern-dependent tunable adhesion in superhydrophobic surfaces by a femtosecond laser. *ACS applied materials & interfaces* **4**, 4905-4912 (2012).
55 Chen, T. *et al.* Biomimetic fabrication of robust self-assembly superhydrophobic surfaces with corrosion resistance properties on stainless steel substrate. *RSC Advances* **6**, 43937-43949 (2016).
56 Brown, M. S. & Arnold, C. B. in *Laser precision microfabrication* 91-120 (Springer, 2010).
57 Long, J. *et al.* Cassie-state stability of metallic superhydrophobic surfaces with various micro/nanostructures produced by a femtosecond laser. *Langmuir* **32**, 1065-1072 (2016).
58 Long, J. *et al.* Superhydrophobic surfaces fabricated by femtosecond laser with tunable water adhesion: from lotus leaf to rose petal. *ACS applied materials & interfaces* **7**, 9858-9865 (2015).
59 Zhu, X., Naumov, A. Y., Villeneuve, D. & Corkum, P. Influence of laser parameters and material properties on micro drilling with femtosecond laser pulses. *Applied Physics A: Materials Science & Processing* **69**, S367-S371 (1999).
60 Wolfe, D. B. *et al.* Customization of Poly (dimethylsiloxane) Stamps by Micromachining Using a Femtosecond-Pulsed Laser. *Advanced Materials* **15**, 62-65 (2003).

61 Meijer, J. Laser beam machining (LBM), state of the art and new opportunities. *Journal of Materials Processing Technology* **149**, 2-17 (2004).
62 Steen, W. M. in *Laser Material Processing* 172-219 (Springer, 1991).
63 Allmen, M. v. & Blatter, A. *Laser-beam interactions with materials: physical principles and applications*. Vol. 2 (Springer Science & Business Media, 2013).
64 Kota, A. K., Li, Y., Mabry, J. M. & Tuteja, A. Hierarchically structured superoleophobic surfaces with ultralow contact angle hysteresis. *Advanced Materials* **24**, 5838-5843 (2012).
65 Tuteja, A., Choi, W., Mabry, J. M., McKinley, G. H. & Cohen, R. E. Robust omniphobic surfaces. *Proceedings of the National Academy of Sciences* **105**, 18200-18205 (2008).
66 Zimmermann, J., Rabe, M., Artus, G. R. J. & Seeger, S. Patterned superfunctional surfaces based on a silicone nanofilament coating. *Soft Matter* **4**, 450-452, doi:10.1039/b717734h (2008).
67 Agble, D. & Mendes-Tatsis, M. A. The prediction of Marangoni convection in binary liquid–liquid systems with added surfactants. *International Journal of Heat and Mass Transfer* **44**, 1439-1449, doi:https://doi.org/10.1016/S0017-9310(00)00159-9 (2001).